Dissecting Contributions to the Thermostability of *Pyrococcus furiosus* Rubredoxin: β-Sheet Chimeras[†]

Marly K. Eidsness,* Kimberly A. Richie, Amy E. Burden, Donald M. Kurtz, Jr., and Robert A. Scott

Department of Chemistry and Center for Metalloenzyme Studies, University of Georgia, Athens, Georgia 30602-2556

Received January 17, 1997; Revised Manuscript Received May 15, 1997[⊗]

ABSTRACT: The contributions to thermostability of interactions within the β-sheet region of rubredoxins (Rds) were investigated by examining proteins in which β-strand sequences of Rds from the hyperthermophilic archaeon *Pyrococcus furiosus* (Pf) and the mesophilic bacterium *Clostridium pasteurianum* (Cp) were interchanged. The thermostabilities of the chimeric Rds were assessed by monitoring the decay of the visible absorbance at 490 nm and of the far-UV CD vs time at 92 °C. The chimeric Rds Pf15|Cp47|Pf (Pf Rd residues 2−15 and 48−54 and Cp Rd residues 16−47) and Cp15|Pf47|Cp were both found to be far less thermostable than wild-type Pf Rd, indicating that neither the β-sheet residues (2−7, 10−15, and 48−53) nor the "core residues" (16−47) of Pf Rd independently confer Pf Rd-like thermostability. However, the chimeric Rd Pf47|Cp exhibits thermostability close to that of wild-type Pf Rd, suggesting that Pf Rd-like thermostability is conferred by interactions of β-sheet strands 1 and 2 (residues 2−15) *together* with Pf core residues. In contrast, Cp Rd β-sheet strands 1 and 2 connecting to Pf Rd core residues are thermodestabilizing in the chimera Cp15|Pf Rd. These results suggest that a global alignment which optimizes both main chain and side chain interactions between β-sheet strands and core residues is more important than a few localized interactions within the β-sheet in conferring Pf Rd-like thermostability.

The molecular determinants of protein thermostability have remained cryptic, despite the isolation and structural characterization of several proteins from hyperthermophilic organisms (Adams & Kelly, 1995; Jaenicke, 1996; Pace et al., 1996). Possible contributions to protein thermostability include hydrophobic packing interactions, van der Waals interactions, hydrogen bonding, and salt bridges. One approach to deconvoluting these interactions is comparing thermostabilizing contributions from secondary structural units, such as α-helices, β-sheets, and loops, in an extremely thermostable protein vs those in a less thermostable analogue. Compared to examining thermostabilizing interactions residue by residue, this approach allows a significant reduction in parameter space.

Here, we report the application of this approach to the β-sheet region of rubredoxin (Rd),[1] a small (53−54 amino acid residues) globular protein with a mononuclear Fe tetrahedrally coordinated to four cysteinyl thiolates. A large body of structural data exists for Rds, including amino acid sequences from more than 15 species, 10 X-ray crystal structures, and an NMR solution structure of Zn-substituted Pf Rd (Blake et al., 1992).

FIGURE 1: Overlay of Cp (blue) and Pf (red) Rd peptide backbones using coordinates from X-ray crystal structures 5rxn and 1caa, respectively (Watenpaugh et al., 1979; Day et al., 1992). β-Sheet regions are shown as arrows, and helical turns are shown as ribbons; the FeS_4 site is shown as a ball and stick, and all other peptide bonds are depicted as coils. The more extensive β-sheet of Pf Rd is observed in all three strands (labeled from N to C termini as 1−3). This figure was generated with the programs MOLSCRIPT (Kraulis, 1991) and Raster3D (Merritt & Murphy, 1994).

The secondary and tertiary structures of Rds are remarkably conserved across hyperthermophilic archaea and mesophilic bacteria, in spite of the vastly different thermostabilities of the proteins (Adams & Kelly, 1995; Richie et al., 1996). A superposition of *Clostridium pasteurianum* Rd (Cp Rd) and *Pyrococcus furiosus* Rd (Pf Rd) peptide backbones is shown in Figure 1. Notable features of all Rd structures include a triple-stranded antiparallel β-sheet consisting of the first 14 or 15 residues of the amino terminus and the

[†] Supported by grants from the National Institutes of Health (GM50736) and the National Science Foundation Research Training Group Award to the Center for Metalloenzyme Studies (DIR 90-14281).

* Address correspondence to this author at the Department of Chemistry, University of Georgia, Athens, GA 30602−2556. E-mail: eidsness@bscr.uga.edu.

[⊗] Abstract published in *Advance ACS Abstracts,* August 15, 1997.

[1] Abbreviations: Rd, rubredoxin; Pf, *Pyrococcus furiosus*; Cp, *Clostridium pasteurianum*; UV, ultraviolet; CD, circular dichroism; PCR, polymerase chain reaction; DNA, deoxyribonucleic acid; FPLC, fast protein liquid chromatography; EPR, electron paramagnetic resonance; Tris, tris(hydroxymethyl)aminomethane; HEPES, 4-(2-hydroxyethyl)piperazine-1-ethanesulfonic acid.

S0006-2960(97)00110-4 CCC: $14.00

FIGURE 2: Amino acid sequences of wild-type and chimeric Rds in order of increasing thermostability from top to bottom. The amino acid residues that participate in β-sheet hydrogen bonds are denoted by arrows for Cp and Pf Rds and labeled 1−3, as in Figure 1. Cp Rd residue numbers are given below the sequences and are used throughout the text for all Rds. The mutations can be tracked visually using the open box (Cp) and shaded box (Pf) coding.

last 5 or 6 residues of the carboxyl terminus (*cf*. Figure 2). In the Pf Rd crystal structure (Day et al., 1992), the residues involved in the main chain hydrogen bond network of the β-sheet are 2−7, 10−15, and 48−53 (see Figure 2 for residue numbering). Figure 1 shows the close proximity of the N-terminal β-sheet strand (1) to the second strand (2) and to the C-terminal strand (3). In comparison, the Cp Rd β-sheet is shortened by one or two residues in each strand (Figures 1 and 2), involving residues 3−7, 11−14, and 48−52 (Watenpaugh et al., 1979). The remaining structure consists of numerous loops and turns, two of which contain the iron ligand pairs Cys 6 and Cys 9 and Cys 39 and Cys 42. Other than the differences in the β-sheet region, the Cp and Pf Rd structures differ only slightly in peptide backbone alignment, and no major structural or spectroscopic differences distinguish the Pf Rd from the Cp Rd, despite the extraordinary thermostability of the former (Blake et al., 1991).

One proposed explanation for the enhanced resistance to thermal denaturation of Pf Rd (Adams & Kelly, 1995) is the more extensive β-sheet network of hydrogen bonds and two salt bridges, one of which includes the unique amino-terminal alanine (Ala 2 in our numbering; *cf*. Figure 2). In Pf Rd, an additional main chain to main chain hydrogen bond forms between the carbonyl oxygen of Ala 2 and the amide nitrogen of Glu 15. In Cp Rd, the analogous residue, Lys 2, is not part of the β-sheet (Watenpaugh et al., 1979). A salt bridge connecting strands 1 and 2 of the β-sheet of Pf Rd is centered on the unique Glu 15. The carboxylate of Glu 15 interacts with the amino-terminal NH_3^+ of Ala 2, the indole nitrogen of Trp 4, and the amide nitrogen of Phe 30. Another residue unique to Pf Rd, Lys 7, forms a second salt bridge between its ϵ-NH_3^+ and the carboxylate of Glu 50, forming a side chain−side chain link between β-sheet strands 2 and 3.

In this work, we have examined the thermostabilities of a series of Cp and Pf Rd β-sheet "chimeras", designed to test the hypothesis which states that the thermostabilizing interactions of Pf Rd lie mainly within the β-sheet region (residues 2−7, 10−15, and 48−53). The underlying premise for these studies is that Pf Rd thermostability is predominantly determined by a few interactions that are significantly weaker or absent in Cp Rd and that these interactions can be transferred intact upon exchanging β-sheet sequences between the two Rds. Thus, Cp Rd amino acid residues in the β-sheet region were mutated to their counterparts in Pf Rd, and vice versa. Figure 2 aligns the sequences of the wild-type and chimeric Rds and indicates the β-sheet regions for Cp and Pf Rds. The chimeric and wild-type Cp and Pf Rd genes were overexpressed in *Escherichia coli*, and the proteins were purified and characterized and their thermostabilities assessed by following the loss of the UV−visible absorbance and far-UV CD spectra upon heating at 92 °C.

EXPERIMENTAL PROCEDURES

Where unspecified, standard molecular biology procedures were followed (Ausubel et al., 1992; Sambrook et al., 1989). *E. coli* strain 71/18 [*supE thiD*(*lac-proAB*) *F′*(*pro-AB* + *lacI*^{q} *LacZ DM15*)] (Messing et al., 1977) was used for initial cloning and amplification of the Rd genes. Cultures were grown aerobically at 37 °C in Luria-Bertani (LB) medium or agar, supplemented with 100 μg/mL ampicillin. The Rd genes were inserted at the *Nde*I and *Hin*dIII restriction sites of plasmid pT7-7 (Tabor, 1990). Nucleotide sequences of all Rd genes were verified by sequencing of both strands in plasmid pT7-7 at the Molecular Genetics Instrumentation Facility (MGIF) at the University of Georgia.

Wild-Type Rd Gene Constructs. The construction and overexpression of the synthetic Cp Rd gene in plasmid pNNQ have been described (Eidsness et al., 1992; Richie et al., 1996; Zeng et al., 1996). A synthetic oligonucleotide encoding the Pf Rd amino acid sequence (Blake et al., 1991) was constructed. Details of the gene construction are given in the Supporting Information.

Chimeric Rd Gene Constructs. The general procedure for constructing all chimeric Rd genes involved PCR site-directed mutagenesis (Ausubel et al., 1992). The template DNA, primer identification, and PCR steps for each Rd

Table 1: Chromatographic Purification Protocols for Rubredoxins

Rd, Fe forms	step	column[a]	flow rate (mL/min)	buffer 1[b]	buffer 2[b]	elution gradient[c]
Cp	1	Mono-Q	2	A	B	23−40% B in 75 mL
	2	Mono-Q	2	A	B	23−33% B in 75 mL
[M1_,K2A,P15E]Cp	1	Mono-Q	2	C	D	20−45% D in 40 mL
	2	Mono-Q	2	C	D	20−45% D in 40 mL
Cp15|Pf47|Cp, Cp15|Pf	1	Mono-Q	2	E	F	15−35% F in 75 mL
	2	Mono-Q	2	E	F	20−30% F in 75 mL
Pf, [_1M]Pf	1	Mono-Q	2	E	F	10−30% F in 75 mL
	2	Mono-Q	2	E	F	20−30% F in 50 mL
	3	CHT1	4	G	H	15−25% H in 150 mL
Pf15|Cp47|Pf	1	Q-Sepharose	4	I	J	20−40% J in 180 mL
	2	Mono-Q	2	A	B	20−40% B in 66 mL
	3	CHT1	4	G	H	15−25% H in 150 mL
Pf47|Cp	1	Mono-Q	2	E	F	15−45% F in 75 mL
	2	Mono-Q	2	E	F	20−30% F in 75 mL
	3	CHT1	4	G	H	15−25% H in 150 mL

[a] Mono-Q, Pharmacia Biotech Mono-Q HR10/10; CHT1, Bio-Rad hydroxyapatite 10 mL; Q-Sepharose, Pharmacia Biotech Q-Sepharose, 30 mL in an XK 16 column. [b] (A) 50 mM Tris-HCl, pH 8.5; (B) A + 1.0 M NaCl; (C) 50 mM Tris-HCl, pH 7.4; (D) C + 1.0 M NaCl; (E) 25 mM Tris-HCl, pH 8.5; (F) E + 1.0 M NaCl; (G) 5 mM sodium phosphate, pH 6.0; (H) 0.5 M sodium phosphate, pH 6.0; (I) 50 mM Tris-HCl, pH 7.5; and (J) I + 1.0 M NaCl. [c] Each elution gradient is preceeded by a step of 0−*X*% buffer 2 in 10 mL, except for the CHT1 column, which was 50 mL, and for the Q-Sepharose column, which was 30 mL, where *X* is the starting percentage of buffer 2 of the elution gradient.

chimera are listed in Table 2 of the Supporting Information. The PCR primer sequences are given in Table 3 of the Supporting Information.

Overexpression and Purification of Rds. *E. coli* strain BL21-DE3 (Novagen, Inc.) containing plasmids with either wild-type or chimeric Rd genes was grown with shaking (250 rpm) or stirring at 37 °C in various volumes (2, 4, or 100 L) of Luria-Bertani medium supplemented with ampicillin (100 or 50 mg/L for 100 L growth), until the optical density at 600 nm reached 1.3−1.5, at which time 0.4 mM (final concentration) isopropyl β-D-thiogalactoside, or 5 mM β-lactose (for 100 L growth), was added. The 100 L growth was inoculated with 4 L of culture (OD_{590} = 1.8) and was carried out at the Fermentation Research Facility at the University of Georgia. The cultures were shaken or stirred for an additional 3 h at 37 °C and then harvested by centrifugation for 20 min at 6000*g*. The cell pellet was resuspended in 50 mL or 1 L (for 100 L growth) of 50 mM Tris-HCl buffer at pH 8.0.

The overexpressed proteins were released from the cells by repeated freeze/thaw cycles (Johnson & Hecht, 1994) or by sonication (550 Sonic Dismembrator, Fisher Scientific). For the 100 L growth, the cells were broken by three passages through a Gaulin homogenizer (APV, Wilmington, MA). The lysates were cleared by centrifugation at 27000*g* for 30 min.

Crude Rd was separated from *E. coli* proteins by passage over a QAE-Sephadex G-25 (Pharmacia Biotech) column, washed with 150 mM NaCl in 50 mM Tris-HCl at pH 8.0, and eluted with 500 mM NaCl in the same Tris buffer. The crude Rd was desalted and concentrated by ultrafiltration in a stirred Amicon cell with a 3000 MWCO membrane.

Purification of Rds was carried out by anion-exchange chromatography on a Mono-Q (Pharmacia Biotech) column connected to a Pharmacia Biotech FPLC system. For some Rds, final purification required passage over a hydroxyapatite column. Overexpression of Rd genes in *E. coli* results in Fe (red) and Zn (colorless) forms of Rd (Richie et al., 1996; Eidsness et al., 1992; Zeng et al., 1996). For a preparative-scale separation of the Fe forms of Rds, the chromatographic procedure is give in Table 1. After purification, the Rds were desalted by ultrafiltration with a YM3 membrane, concentrated in YM3 Centricon tubes (Amicon), and stored at 4 or −80 °C.

Characterization of Rds. UV−visible absorption spectra were recorded on a Shimadzu UV-2101PC scanning spectrophotometer, using 1 cm path length quartz cuvettes. The Fe-containing Rds were characterized by their UV−visible absorption spectra, metal analysis [performed by inductively coupled plasma atomic emission (ICP-AE) spectrometry at the Chemical Analysis Laboratory at the University of Georgia], EPR spectra (recorded at a liquid helium temperature on a Bruker ESP-300E spectrometer equipped with an ER-4116 dual-mode cavity and an Oxford Instrument ESR-9 flow cryostat), and electrospray ionization mass spectrometry (at the Chemical and Biological Sciences Mass Spectrometry facility by D. Phillips). Experimental and calculated molecular weights of all Rds are given in Table 4 of the Supporting Information.

Thermostability Measurements with UV−Visible Absorbance Decay. Fe Rds were buffer exchanged into water and their concentrations determined by 280 nm absorbance (ϵ_{280} = 21 300 M^{-1} cm^{-1}) (Lovenberg & Walker, 1978) for Cp, [M1_,K2A,P15E]Cp, and Pf15|Cp47|Pf Rds and 490 nm absorbance (ϵ_{490} = 9220 M^{-1} cm^{-1}) (Blake et al., 1991) for Cp15|Pf47|Cp, Pf47|Cp, Cp15|Pf, [_1M]Pf, and Pf Rds. For thermostability studies, the Rd concentration was 35 μM and the buffer concentration was 50 mM HEPES at pH 8.2 (at room temperature). While no attempt was made to exclude air, the samples were sealed in a 1 mL quartz cuvette with a Teflon cap and allowed to reach temperature equilibrium for 15 min before UV−visible absorbance measurements commenced. Spectra were recorded at specific time intervals, until the absorbance at 490 nm decayed completely, or until 88 h passed. The temperature was controlled by a VWR 1160 bath filled with 50% ethylene glycol, and the temperature of the sample compartment was monitored by an RTD element (Omega Engineering, Inc.) placed next to the cuvette and connected to a digital display (Omega RTD model 199). The temperature of the sample cuvette holder was 92 ± 1 °C.

UV−visible absorption time courses were analyzed by plotting the fractional loss of visible absorbance at 490 nm

vs time at 92 °C. The fractional absorbance was calculated by subtracting the final 490 nm absorbance (A_f) from the absorbance at time t (A_t) and dividing this number by the initial absorbance (A_i) minus the final absorbance $[(A_t - A_f)/(A_i - A_f)]$. This calculation was adjusted for Pf Rd and [_1M]Pf by plotting only $(A_t - A_{t700})/(A_i - A_{i700})$, because A_f was never attained in these cases. For these samples, absorbance at 700 nm was subtracted to correct for spectrophotometer drift over the extended periods of data collection. The time required for loss of the 490 nm absorbance is reported as −1/slope of a line fit to the decay data for each Rd.

Thermostability Measurements with Far-UV CD. Far-UV circular dichroism (CD) spectra were measured at room temperature on a Jasco 710 CD spectrophotometer, using a 1 mm path length cylindrical quartz cuvette, with nitrogen gas (research-grade) flowing in the sample compartment. Six or more scans were averaged for each sample. The CD spectra were obtained on aliquots removed from the cuvettes during the visible absorbance decay studies and immediately frozen at −80 °C until recording of the CD spectra. CD spectra were obtained on freshly thawed aliquots which had been removed before heating, at a specified time after the visible absorbance had decayed, and after complete decay of the visible absorbance with heating. The CD spectra of samples that were never frozen were indistinguishable from those of samples that were frozen and thawed one time, and no samples were frozen and thawed more than one time.

RESULTS

Description of Rd Chimeras

The following Rd chimeras (whose amino acid sequences are shown in Figure 2) have been constructed, overexpressed, and characterized: [M1_,K2A,P15E]Cp, Pf15|Cp47|Pf, Cp15|Pf47|Cp, Cp15|Pf, Pf47|Cp, and [_1M]Pf Rds. The shorthand nomenclature describes the amino acid sequence of each chimera. Point mutations are listed in brackets explicitly; vertical lines represent a switch from Pf to Cp sequences (or vice versa) at the amino acid number following the one given, and Pf or Cp designation to the right of the vertical line (or bracket) represents the remaining amino acid sequence of wild-type Pf or Cp Rd. The underline character in [M1_,K2A,P15E]Cp and [_1M]Pf Rds indicates the absence of a residue in that position; in the former, M1 is removed, and in the latter, M1 is added. The mutations can be tracked visually by following the coding in Figure 2.

[M1_,K2A,P15E]Cp. This chimera lacks the N-terminal Met of wild-type Cp Rd, and the K2A mutation (using Cp Rd amino acid numbering) makes its N-terminal alanine match that of Pf Rd. The P15E mutation introduces the carboxylate side chain that, in Pf Rd, forms a salt bridge with the amino-terminal nitrogen of Ala 2 and a hydrogen bond with the amide group of Phe 30.

Pf15|Cp47|Pf. This chimeric Rd duplicates all of the amino acid residues in the β-sheet region of Pf Rd. Its sequence matches that of Pf Rd residues 2−15 and 48−54 and Cp Rd residues 16−47. The additional mutations in Pf15|Cp47|Pf beyond those in [M1_,K2A,P15E]Cp are Y4W, T5V, T7K, V8I, N14D, Q48E, E51I, V52L, and E54D. These additional mutations introduce all of the residues involved in the Glu 15-centered hydrogen bond/salt bridge network and the Lys 7 side chain to side chain hydrogen bond with Glu 50. The V8I and N14D mutations were made to match the Pf Rd amino acid sequence, although no specific interactions involving these residues are apparent in the Pf Rd structure.

Cp15|Pf47|Cp. This chimera is essentially the complement of Pf15|Cp47|Pf. The residues involved in the β-sheet hydrogen bonds in Pf Rd have been replaced with the analogous residues from Cp Rd. It is composed of Cp Rd amino acid residues 1−15 and 48−54 and Pf Rd residues 16−47.

Cp15|Pf. This chimera duplicates the Pf Rd sequence for residues 16−54 and the Cp Rd sequence for residues 1−15. Thus, β-sheet strands 1 and 2 display the Cp Rd sequence, and strand 3 displays the Pf Rd sequence (see Figure 1).

Pf47|Cp. The amino acid sequence of this chimera duplicates Pf Rd residues 2−47 and Cp Rd residues 48−54. Thus, β-sheet strands 1 and 2 are from Pf Rd, and strand 3 is from Cp Rd.

[_1M]Pf. This mutant duplicates the wild-type Pf Rd amino acid sequence but with the addition of an N-terminal methionine. The [_1M]Pf and the formyl[_1M]Pf Rds were obtained along with wild-type Pf Rd upon overexpression of the Pf Rd gene in *E. coli*. These N-terminally modified products presumably arise from incomplete processing of overexpressed Pf Rd by the deformylase and methionyl aminopeptidase of *E. coli* (Ben-Bassat et al., 1987; Dalbøge et al., 1990; Hirel et al., 1989; Meinnel et al., 1993).

Characterization of Rd Chimeras

The UV−visible absorbance ratios of A_{280}/A_{490} for recombinant wild-type Cp Rd, Pf Rd, and the Fe(III) Rd chimeras were found to be close to the published absorbance ratios, 2.4, for Cp Fe(III) Rd isolated originally from *C. pasteurianum* (Lovenberg & Walker, 1978), and 2.78, for Pf Fe(III) Rd isolated from *P. furiosus* (Blake et al., 1991). Oxidized [*i.e.* Fe(III)] Rd has a distinctive UV−visible absorption spectrum, with an intense band at 280 nm and bands at 385 and 490 nm, ascribed to charge transfer transitions from cysteinyl thiolate to Fe(III) (Eaton & Lovenberg, 1973; Lowery et al., 1993). The EPR spectra (data not shown) of recombinant wild-type Fe(III) Pf, Cp, and chimeric Rds are all very similar to each other, exhibiting g values of 9.6 and 4.3. The insignificant changes observed in the thiolate → Fe(III) charge transfer transitions (in the visible spectrum) and the EPR g values suggest that the electronic properties of the Fe(III) sites are essentially unchanged in the recombinant wild-type and chimeric Rds. ICP-AE analyses confirmed that the Rds contained 1.0 mol of Fe/(mol of Rd). Molecular weights of Rds were determined by electrospray ionization mass spectrometry (ESI-MS) and are listed in Table 4 of the Supporting Information. In all cases, the ESI-MS molecular weight determinations agreed with calculated molecular weights within experimental error (0.1%).

Rubredoxin Thermostabilities

The relative thermostabilities of the wild-type and chimeric Rds were assessed by following the loss of visible absorbance as a function of time at 92 °C. This process is illustrated for wild-type Cp and Pf Rds in Figure 3. In the experiments described here, the loss of visible absorbance is not due to

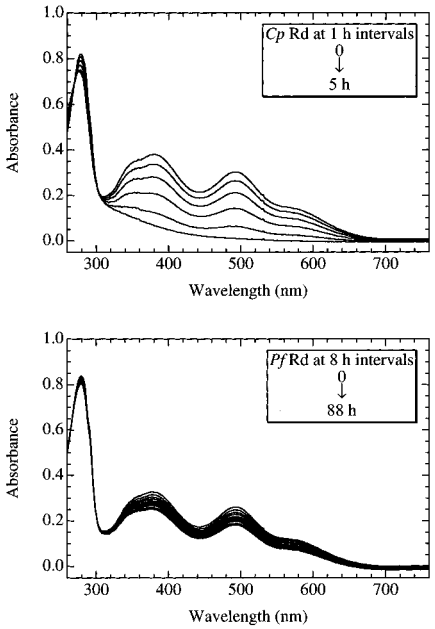

FIGURE 3: Decay of Cp (top) and Pf (bottom) Rd visible absorbance vs time at 92 °C. Cp and Pf Rd concentrations were 35 μM in 50 mM HEPES at pH 7.8 and 92 °C (at 25 °C and pH 8.2). The Cp Rd absorbance was recorded at 1 h intervals for 5 h, and the Pf Rd absorbance was recorded at 8 h intervals for 88 h.

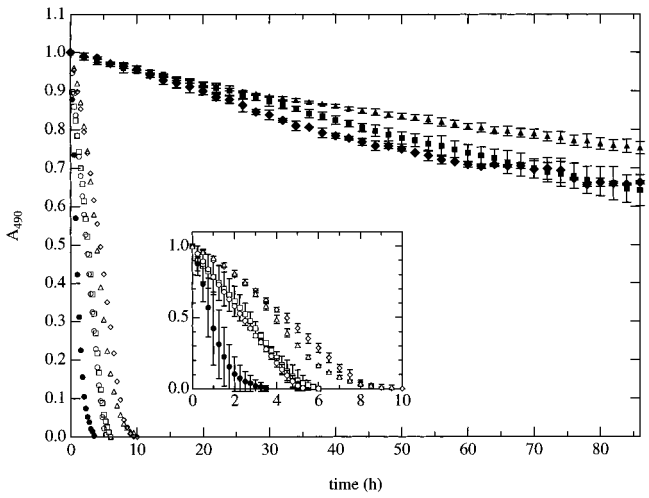

FIGURE 4: Cp, Pf, and chimeric Rd 490 nm absorbance decays vs time at 92 °C: Cp15|Pf (●), M1_,K2A,P15E]Cp (○), Cp Rd (□), [Cp15|Pf47|Cp (△), Pf15|Cp47|Pf (◇), [_1M]Pf Rd (■), Pf47|Cp (◆), and Pf Rd (▲). The data are the average of two measurements for each sample, and standard deviations are given as error bars. The inset is an enlargement of the decay data for all samples except Pf, [_1M]Pf, and Pf47|Cp Rds. Rd concentrations were 35 μM, and the buffer was 50 mM HEPES at pH 7.8 and 92 °C (at 25 °C and pH 8.2).

simple reduction of the $Fe(SCys)_4$ center from Fe(III) to Fe(II), because the characteristic 311 and 333 nm features of the Fe(II) Rd are not observed. Rather, the loss of visible absorbance is apparently due to the loss of the native structure of the iron−sulfur center upon incubation at 92 °C. Proteins that underwent a complete bleaching of spectral features at 385 and 490 nm remained free of detectable precipitate, indicating that insoluble ferric oxides or proteins did not form.

For those Rds whose A_{490} disappeared completely upon heating at 92 °C, cooling to room temperature afforded negligible recovery of the native Fe(III) site, even after incubation for days. Thus, these measurements apparently monitor an irreversible process which includes Fe(III) site degradation and protein unfolding (the latter monitored by CD, vide infra). However, both Pf and [_1M]Pf Rds exhibited significant recovery of A_{490} at room temperature after ∼30% degradation of the visible absorbance (∼100 h at 92 °C). Other Rd chimeras also showed this reversibility when thermally degraded to the same fractional extent (∼30% loss of A_{490}), suggesting similar decay processes in all of the Rds examined.

The times required for degradation of the iron sites in these Rds, as measured by the fractional loss of 490 nm absorbance at 92 °C, are compared in Figure 4. Although we have so far been unable to fit the absorbance decay curves to those expected for simple zero- or first-order kinetic processes, estimates of the A_{490} lifetimes can be obtained by linear least-squares fits to the A_{490} decay. The negative inverse of the slopes of these fits approximates the times required for complete loss of A_{490} of the various Rds; these values are provided in Table 2.

The loss of 490 nm absorbance of wild-type Cp Rd is complete in ca. 6 h at 92 °C, as is that of the [M1_,K2A,P15E]Cp Rd. The Pf15|Cp47|Pf Rd visible absorbance decays completely in ca. 9 h at 92 °C, and the Cp15|Pf47|Cp chimera is only slightly less stable. Although incorporation of Pf Rd β-sheet strands 1−3 into Cp Rd (the Pf15|Cp47|Pf mutations) has increased the A_{490} lifetime at 92 °C by a factor of 1.6 relative to that of wild-type Cp Rd, this chimera remains much less thermostable than wild-type Pf or [_1M]-Pf Rds (whose lifetimes are estimated to be ∼380 and ∼240 h, respectively, at 92 °C, Table 2). In contrast, the Cp15|Pf47|Cp chimera shows a dramatic decrease in thermostability compared to that of wild-type Pf Rd. The Cp15|Pf Rd visible absorbance decays completely in 4 h, making it the least stable of all Rds examined. In contrast, the Pf47|Cp chimera is similar in thermostability to wild-type Pf and [_1M]Pf Rds, all of whose A_{490} lifetimes at 92 °C exceed 230 h.

The thermostability of the Rd secondary structure was monitored by recording far-UV circular dichroism (CD) spectra at room temperature of Rd samples removed at various times during the 92 °C incubations. These far-UV CD spectra for wild-type Cp and Pf Rds and Pf15|Cp47|Pf Rd are shown in Figure 5. In all cases except for wild-type Pf and [_1M]Pf Rds, the positive ellipticity at 195 nm and negative ellipticity at 202 and 226 nm, associated with β-sheet in Rds (Christensen et al., 1994), lost intensity after heating at 92 °C and were replaced by a negative ellipticity centered around 202 nm, associated with random coil configurations.

The wild-type Cp Rd CD spectral changes continued for 12 h, in contrast to the total loss of visible absorbance in ca. 6 h. The CD spectrum of wild-type Cp Rd after heating for 6 h at 92 °C showed a strong negative ellipticity at 202 nm and a weaker negative ellipticity at 226 nm. Apparently, Cp Rd retains secondary structure for a number of hours after the metal site has been destroyed, but eventually (12 h) reverts to a random coil. Similarly, the Pf15|Cp47|Pf and Cp15|Pf47|Cp chimeras showed loss of negative ellipticity at 225 nm after 9 h of heating 92 °C, at which point the visible absorbance is gone, and lost the remaining negative ellipticity at 226 nm after 10 h of additional heating at 92 °C. The far-UV CD spectra of wild-type Pf and [_1M]Pf

Table 2: Summary of Estimated A_{490} Lifetimes at 92 °C for Each Rd

Rd	lifetime[a] (h)	species: amino acid residues 1−15	species: amino acid residues 16−47	species: amino acid residues 48−54	interaction[b] I	interaction[b] II
Cp15|Pf	3.6	Cp	Pf	Pf		
[M1_,K2A,P15E]Cp	5.5	Cp[c]	Cp	Cp		x
Cp	5.8	Cp	Cp	Cp		x
Cp15|Pf47|Cp	8.3	Cp	Pf	Cp		x
Pf15|Cp47|Pf	8.9	Pf	Cp	Pf		x
[_1M]Pf	240	Pf[c]	Pf	Pf	x	
Pf47|Cp	250	Pf	Pf	Cp	x	
Pf	380	Pf	Pf	Pf	x	x

[a] Estimated from the negative inverse of the slope of linear least-squares fits to the 490 nm absorbance decays vs time at 92 °C for each Rd shown in Figure 4. [b] Intramolecular interactions. I is the proposed dominant interaction of Pf residues [(1−15)−(16−47)]; II is the potentially naturally occurring set of intra-β-sheet interactions [(1−15)−(48−54)], either Pf or Cp residues. [c] These species contain point mutations.

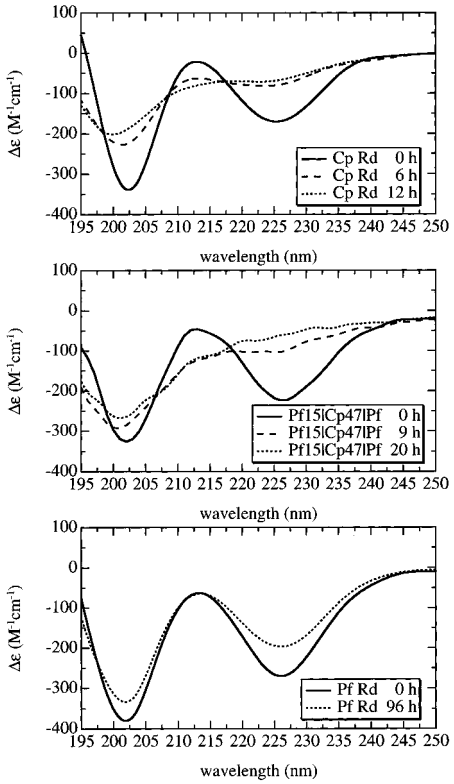

FIGURE 5: Far-UV CD of Cp (top), Pf15|Cp47|Pf (middle), and Pf (bottom) Rds at room temperature before heating (solid line) and after heating at 92 °C for 6 and 9 h (dashed line) for Cp and Pf15|Cp47|Pf Rds, respectively, and after 12, 20, and 96 h for Cp, Pf15|Cp47|Pf, and Pf Rds, respectively (dotted line). Rd concentrations were 3.5 μM, and the buffer was 5 mM HEPES at pH 8.2.

Rds, after heating at 92 °C for 96 h, retained negative ellipticities at 202 and 226 nm, indicating persistence of the β-sheet structure in these Rds, which is consistent with the partial loss of visible absorbance shown in Figures 3 and 4.

DISCUSSION

As indications of the relative thermal stabilities of the wild-type and chimeric Rds, we have monitored the thermally induced disappearance of spectral features associated with the native Fe(III) site (A_{490}) and with β-sheet secondary structure (θ_{225}). Although our CD measurements indicate a continued loss of secondary structure after disappearance of A_{490}, in most cases, the overall CD lifetimes were approximately twice the A_{490} lifetimes so that both spectroscopies measured the same *relative* thermostabilities at 92 °C. For wild-type Pf and [_1M]Pf Rds, this correlation could not be confirmed since A_{490} was never followed to complete disappearance (our spectrophotometer baseline was found to be unstable over the several weeks that would be required for such measurements at 92 °C). While the heat-induced partial decay (up to ca. 30%) of these absorption spectra could be reversed upon room-temperature incubation, the completely decayed absorption spectra could not be so reversed.

The thermostabilities of the various wild-type and chimeric Rds are compared in terms of A_{490} lifetimes at 92 °C, which are listed in Table 2. For purposes of discussion, the wild-type and chimeric Rds can be divided into two main thermostability groups (*cf.* Figure 4 and Table 2): wild-type Cp, [M1_,K2A,P15E], Cp15|Pf47|Cp, Pf15|Cp47|Pf, and Cp15|Pf with A_{490} lifetimes of 4−9 h and wild-type Pf, [_1M]-Pf, and Pf47|Cp with (estimated) A_{490} lifetimes of 240−380 h.

The heat denaturation we observe in the less stable groups of Rds is presumably kinetically driven, since the process is irreversible. Kinetically based thermal decay mechanisms for Rds could include covalent modifications, such as oxidation of amino acid side chains and peptide backbone cleavage, some of which may be iron- and/or O_2-catalyzed (since no attempt was made to exclude O_2 in these studies). However, regardless of the mechanism(s) for thermal denaturation, the data in Figure 4 and Table 2 indicate that the kinetic barriers to irreversible denaturation of Pf Rd must be much higher than those of Cp Rd. This investigation set out to test the hypothesis which states that these kinetic barriers arise from unique interactions within the β-sheet of Pf Rd.

We now discuss possible contributions to the relatively high thermostability of wild-type Pf, [_1M]Pf, and Pf47|Cp Rds on the basis of our results.

Glu 15 H Bond/Salt Bridge Network. A unique network of hydrogen bonds and salt bridges in Pf Rd is centered on the carboxylate side chain of Glu 15. The oxygen atoms of this carboxylate serve as acceptors for H bonds with the indole nitrogen of Trp 4 and the main chain amide of Phe 30 and form a salt bridge with the N-terminal amino group (on Ala 2). In Cp Rd, the substitution of Pro 15, the extension of the N terminus by the addition of Met, and the W4Y substitution all preclude formation of this H bond network. The [M1_,K2A,P15E]Cp Rd was designed to test the ability of a major part of this H bond network to confer thermostability when engineered into Cp Rd. Multidimensional NMR studies of Zn-substituted [M1_,K2A,P15E]Cp

Rd (Richie et al., 1996) confirm the expected extension of the first two strands of β-sheet to include Ala 2 and Glu 15 even in the absence of Trp 4. However, the incorporation of these additional H bonds does not significantly increase the thermostability of Cp Rd (A_{490} lifetime of 5.5 h for [M1_,-K2A,P15E]Cp compared to 5.8 h for the wild type, Figure 4 and Table 2). Additional Y4W substitution (among others) in [P15E]Pf7|Cp Rd does not alter this result (Elkin, 1995). We therefore conclude that the Glu 15-centered H bond/salt bridge network is not by itself the predominant determinant of Pf Rd thermostability.

N Terminus. The unique Ala 2 has been proposed to be a significant determinant of Pf Rd thermostability (Blake et al., 1992). However, we found that neutralization of the Ala 2 NH_3^+ by incorporation of Met 1 in the Pf Rd variant [_1M]-Pf Rd only marginally destabilizes Pf Rd toward heat (Figure 4). This mutation eliminates the salt bridge between the Glu 15 carboxylate and the N-terminal NH_3^+ of Ala 2 (although a hydrogen bonding interaction with the neutral amide of the Ala 2 is still possible). Thus, salt bridges involving the unique N-terminal Ala 2 amino group do not appear to be a significant contributor to the thermostability of Pf Rd.

Contribution of the β-Sheet. The Cp15|Pf47|Cp chimeric Rd incorporates Cp Rd sequence in all three strands of the β-sheet, but Pf Rd sequence elsewhere (Figure 2). This chimera is only 1.6 times more stable than wild-type Cp Rd (as measured by the A_{490} lifetime) and exhibits much lower thermostability than Pf Rd (Figure 4). This result shows that substitution of the Pf Rd β-sheet sequences with the corresponding Cp Rd sequences drastically reduces Pf Rd thermostability and, if taken by itself, implies that the β-sheet region *does* contain the predominant determinant of Pf Rd thermostability. However, caution must be exercised in drawing such conclusions, since the complementary chimera, Pf15|Cp47|Pf, shows similarly low thermostability (Figure 4), suggesting that the three-stranded β-sheet does *not* contain the predominant determinant of Pf Rd thermostability. Two-dimensional ^1H and three-dimensional $^1H-^{15}N$ NMR studies of these two chimeras indicate that the transferred β-sheet structures are essentially intact at least up to 35 °C (K. A. Richie, Q. Teng, and D. M. Kurtz, Jr., unpublished results). In fact, the relatively low thermostabilities of the two complementary chimeric Rds establish the fact that neither the Pf Rd β-sheet region nor the Pf Rd core region (residues 16−47) contains independent sets of interactions sufficient to confer Pf Rd-like thermostability. Thus, if there are localized interactions (H bonds, salt bridges, or hydrophobic packing) in Pf Rd that dominate thermostabilization, these results would suggest that they exist at the interface of the β-sheet and core structural elements, and this β-sheet/core interface of Pf Rd is not reconstructed in either Pf15|Cp47|Pf or Cp15|Pf47|Cp chimeras.

To further investigate this possibility, two additional chimeric Rds were constructed. One chimera, Cp15|Pf, consists of β-sheet strands 1 and 2 of the Cp Rd sequence combined with the remaining Pf Rd sequence (residues 16−54). The second chimera, Pf47|Cp, consists of Cp Rd β-sheet strand 3 grafted onto the remaining Pf Rd sequence (residues 2−47). Incorporation of the Pf Rd β-sheet strand 3 into Cp15|Pf47|Cp results in the Cp15|Pf Rd chimera, which exhibits a surprising *reduction* in thermostability (A_{490} lifetime of 3.6 h for Cp15|Pf compared to 8.3 h for Cp15|Pf47|Cp Rd, Figure 4). This result suggests that any stabilizing interactions between the introduced Pf Rd β-sheet strand 3 (residues 48−54) and the Pf sequence core (residues 16−47) are more than offset by additional destabilizing interactions between each of those two regions and Cp Rd β-sheet strands 1 and 2.

In contrast to the results observed for Cp15|Pf, substitution of Pf Rd strands 1 and 2 of the β-sheet into Cp15|Pf47|Cp to generate Pf47|Cp Rd restores nearly all of the wild-type Pf Rd thermostability (Figure 4). This result suggests the existence of particularly strong stabilizing interactions between Pf Rd β-sheet strands 1 and 2 (residues 2−15) and the Pf Rd core (residues 16−47) that are not mimicked or compensated for by Cp Rd β-sheet strands 1 and 2 (in Cp15|Pf47|Cp). In Pf47|Cp (and Pf) Rd, the thermostabilizing interactions may include the hydrogen bond linking Pf Rd β-sheet strand 2 to the Pf Rd core through the Phe 30 main chain amide to the Glu 15 side chain carboxylate; Cp Rd β-sheet strand 2 with Pro 15 lacks this hydrogen bond. Hydrophobic interactions may also contribute to Pf Rd thermostability but are difficult to evaluate.

CONCLUSIONS

The measurement of relative thermostabilities of Pf/Cp chimeric Rds allows the following conclusions to be drawn.

(1) Neither the unique H bond network centered on the Glu 15 side chain nor salt bridges on the shortened N terminus can by themselves account for the increased thermostability of Pf Rd with respect to that of Cp Rd.

(2) Neither the β-sheet (residues 2−15 and 48−54) nor the core (residues 16−47) of Pf Rd contains independent sets of interactions which control overall thermostability, suggesting the existence of thermostabilizing interactions *between* the core and β-sheet.

(3) Substitution of Cp Rd β-sheet strands 1 and 2 into Pf Rd has a large thermodestabilizing effect. By contrast, substitution of Cp Rd β-sheet strand 3 into Pf Rd has very little effect on Pf Rd thermostability.

These results narrow the search for thermostabilizing interactions of Pf Rd to those between the core (residues 16−47) and β-sheet strands 1 and 2 (residues 2−15). This set of interactions is labeled I in Table 2. Two unique salt bridges have been reported within this region: Glu 15 OE1 to Ala 2 (amino terminus) (2.78 Å) and Lys 7 NZ to Glu 50 OE1 (4.21 Å). However, in the two chimeric Rds with thermostability only 1.6 times greater than that of Cp Rd, Pf15|Cp47|Pf Rd can potentially have both salt bridges, whereas Cp15|Pf47|Cp Rd can have neither. Thus, these data do not suggest a correlation between the number of potential salt bridges and thermostability. These observations agree with an earlier study on Pf Rd at pH 2 (Cavagnero et al., 1995), which suggested that electrostatic interactions are not the dominant factor affecting thermostability. Hydrogen bonding and hydrophobic interactions remain as potentially dominant contributors to thermostability of Pf Rd. Since our results do not identify a few dominant localized interactions, we suggest that the extraordinary thermostability of Pf Rd may involve a precise, optimal alignment of a large number of residues, whose network of interactions are very sensitive to small structural changes dictated by the context of the sequence. Thus, slight misalignment of the β-sheet strands 1 and 2 vs core residues in the chimeric Rds would explain their vastly decreased thermostabilities. This pro-

posal implies a more global view of thermostability, in which the strengthening of many small interactions (via realignment of one substructure with a neighboring one) results in a large increase in thermostability.

SUPPORTING INFORMATION AVAILABLE

Pf Rd synthetic gene construction, oligonucleotide sequences, Rd chimeric gene templates, primer sequences, PCR steps, and molecular weight determinations of Rds by ESI mass spectrometry (7 pages). Ordering information is given on any current masthead page.

REFERENCES

Adams, M. W. W., & Kelly, R. M. (1995) *Chem. Eng. News 73*, 32−42.

Ausubel, F. M., Brent, R., Kingston, R. E., Moore, D. D., Seidman, J. G., Smith, J. A., & Struhl, K. (1992) in *Current Protocols in Molecular Biology*, Wiley, New York.

Ben-Bassat, A., Bauer, K., Chang, S.-Y., Myambo, K., Boosman, A., & Chang, S. (1987) *J. Bacteriol. 169*, 751−757.

Blake, P. R., Park, J.-B., Bryant, F. O., Aono, S., Magnuson, J. K., Eccleston, E., Howard, J. B., Summers, M. F., & Adams, M. W. W. (1991) *Biochemistry 30*, 10885−10895.

Blake, P. R., Park, J.-B., Zhou, Z. H., Hare, D. R., Adams, M. W. W., & Summers, M. F. (1992) *Protein Sci. 1*, 1508−1521.

Cavagnero, S., Zhou, Z. H., Adams, M. W. W., & Chan, S. I. (1995) *Biochemistry 34*, 9865−9873.

Christensen, H. E. M., Hammerstad-Pedersen, J. M., Holm, A., Iversen, G., Jensen, M. H., & Ulstrup, J. (1994) *Eur. J. Biochem. 224*, 97−101.

Dalbøge, H., Bayne, S., & Pedersen, J. (1990) *FEBS Lett. 266*, 1−3.

Day, M. W., Hsu, B. T., Joshua-Tor, L., Park, J.-B., Zhou, Z. H., Adams, M. W. W., & Rees, D. C. (1992) *Protein Sci. 1*, 1494−1507.

Eaton, W. A., & Lovenberg, W. (1973) in *Iron-Sulfur Proteins* (Lovenberg, W., Ed.) pp 131−162, Academic Press, New York.

Eidsness, M. K., O'Dell, S. E., Kurtz, D. M., Jr., Robson, R. L., & Scott, R. A. (1992) *Protein Eng. 5*, 367−371.

Elkin, C. J. (1995) M.S. Thesis, University of Georgia, Athens, GA.

Hirel, P.-H., Schmitter, J.-M., Dessen, P., Fayat, G., & Blanquet, S. (1989) *Proc. Natl. Acad. Sci. U.S.A. 86*, 8247−8251.

Jaenicke, R. (1996) *FASEB J. 10*, 84−92.

Johnson, B. H., & Hecht, M. H. (1994) *Bio/Technology 12*, 1357−1360.

Kraulis, P. (1991) *J. Appl. Crystallogr. 24*, 946−950.

Lovenberg, W., & Walker, M. N. (1978) *Methods Enzymol. 53*, 340−346.

Lowery, M. D., Guckert, J. A., Gebhard, M. S., & Solomon, E. I. (1993) *J. Am. Chem. Soc. 115*, 3012−3013.

Meinnel, T., Mechulam, Y., & Blanquet, S. (1993) *Biochimie 75*, 1061−1075.

Merritt, E. A., & Murphy, M. E. P. (1994) *Acta Crystallogr. D 50*, 869−873.

Messing, J., Gronenborn, B., Müller-Hill, B., & Hofschneider, P. H. (1977) *Proc. Natl. Acad. Sci. U.S.A. 74*, 3642−3646.

Pace, C. N., Shirely, B. A., McNutt, M., & Gajiwala, K. (1996) *FASEB J. 10*, 75−83.

Richie, K. A., Teng, Q., Elkin, C. J., & Kurtz, D. M., Jr. (1996) *Protein Sci. 5*, 883−894.

Sambrook, J., Fritsch, E. F., & Maniatis, T. (1989) in *Molecular Cloning: A Laboratory Manual, 2nd ed.*, Cold Spring Harbor Laboratory Press, Plainview, NY.

Tabor, S. (1990) in *Current Protocols in Molecular Biology* (Ausubel, F. A., Brent, R., Kingston, R. E., Moore, D. D., Seidman, J. G., Smith, J. A., & Struhl, K., Eds.) pp 16.2.1−16.2.11, Greene Publishing and Wiley-Interscience, New York.

Watenpaugh, K. D., Sieker, L. C., & Jensen, L. H. (1979) *J. Mol. Biol. 131*, 509−522.

Zeng, Q., Smith, E. T., Kurtz, D. M., Jr., & Scott, R. A. (1996) *Inorg. Chim. Acta 242−243*, 245−251.

BI970110R